

Weakly-Supervised Reinforcement Learning for Controllable Behavior

Lisa Lee^{1,2} Benjamin Eysenbach^{1,2} Ruslan Salakhutdinov¹ Shixiang (Shane) Gu² Chelsea Finn^{2,3}

Abstract

Reinforcement learning (RL) is a powerful framework for learning to take actions to solve tasks. However, in many settings, an agent must winnow down the inconceivably large space of all possible tasks to the single task that it is currently being asked to solve. Can we instead constrain the space of tasks to those that are semantically meaningful? In this work, we introduce a framework for using weak supervision to automatically disentangle this semantically meaningful subspace of tasks from the enormous space of nonsensical “chaff” tasks. We show that this learned subspace enables efficient exploration and provides a representation that captures distance between states. On a variety of challenging, vision-based continuous control problems, our approach leads to substantial performance gains, particularly as the complexity of the environment grows.

1. Introduction

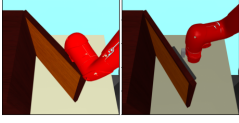
A general purpose agent must be able to efficiently learn a diverse array of tasks through interacting with the real world. The typical approach is to manually define a set of reward functions and only learn the tasks induced by these reward functions (Finn et al., 2017; Hausman et al., 2018). However, defining and tuning the reward functions is labor intensive and places a significant burden on the user to specify reward functions for all tasks that they care about. Designing reward functions that provide enough learning signal yet still induce the correct behavior at convergence is challenging (Hadfield-Menell et al., 2017). An alternative approach is to parametrize a family of tasks, such as goal-reaching tasks, and learn a policy for each task in this family (Hazan et al., 2018; Pong et al., 2019; Lee et al., 2019b; Ghasemipour et al., 2019; Stanley & Miikkulainen, 2002; Pugh et al., 2016). However, learning a single goal-conditioned policy for reaching all goals is a challenging optimization problem and is prone to underfitting, especially in high-dimensional tasks with limited data (Dasari et al.,

2019). In this work, we aim to accelerate the acquisition of goal-conditioned policies by narrowing the goal space through weak supervision. Answering this question would allow an RL agent to prioritize exploring and learning meaningful tasks, resulting in faster acquisition of behaviors for solving human-specified tasks.

How might we constrain the space of tasks to those that are semantically meaningful? Reward functions and demonstrations are the predominant approaches to training RL agents, but they are expensive to acquire (Hadfield-Menell et al., 2017). Generally, demonstrations require expert humans to be present (Finn et al., 2016a; Duan et al., 2017; Laskey et al., 2017), and it remains a challenge to acquire high-quality demonstration data from crowdsourcing (Mandlekar et al., 2018). In contrast, human preferences and ranking schemes provide an interface for sources of supervision that are easy and intuitive for humans to specify (Christiano et al., 2017), and can scale with the collection of offline data via crowd-sourcing. However, if we are interested in learning many tasks rather than just one, these approaches do not effectively facilitate scalable learning of many different tasks or goals.

In this work, we demonstrate how weak supervision provides useful information to agents with minimal burden, and how agents can leverage that supervision when learning in an environment. We will study one approach to using weak supervision in the goal-conditioned RL setting (Kaelbling, 1993; Schaul et al., 2015; Andrychowicz et al., 2017; Pong et al., 2018; Nair et al., 2018). Instead of exploring and learning to reach every goal state, our weakly-supervised agent need only learn to reach states along meaningful axes of variation, ignoring state dimensions that are irrelevant to solving human-specified tasks. Critically, we propose to place such constraints through weak forms of supervision, instead of enumerating goals or tasks and their corresponding rewards. This weak supervision is obtained by pairwise queries (see Figure 1), and our approach uses this supervision to learn a structured representation space of observations and goals, which can in turn be used to guide exploration, goal generation, and learning. Our approach enables the user to specify the axes of variation that matter for the efficient development of general-purpose agents, and implicitly characterize factors that are not relevant to human-specified tasks.

¹Carnegie Mellon University ²Google Brain ³Stanford University. Correspondence to: Lisa Lee <lsllee@cs.cmu.edu>.



In which image...

1. ...is the door opened wider?
2. ...is the lighting brighter?
3. ...is the robot closer to the door?

Figure 1: We propose weak supervision as a means to scalably introduce structure into goal-conditioned RL. The weak supervision is provided by a human who answers true/false questions (right) based on the two images (left).

The main contribution of this work is *weakly-supervised control* (WSC), a simple framework for introducing weak supervision into RL. Our approach learns a semantically meaningful representation space with which the agent can generate its own goals, acquire distance functions, and perform directed exploration. WSC consists of two stages: we first learn a disentangled representation of states from weakly-labeled offline data, then we use the disentangled representation to constrain the exploration space for RL agents. We empirically show that learning disentangled representations can speed up reinforcement learning on various manipulation tasks, and improve the generalization abilities of the learned RL agents. We also demonstrate that WSC produces an *interpretable* latent policy, where latent goals directly align with controllable features of the environment.

2. Preliminaries

In this section, we overview notation and prior methods that we build upon in this work.

2.1. Goal-conditioned reinforcement learning

We define a finite-horizon goal-conditioned Markov decision process by a tuple $(\mathcal{S}, \mathcal{A}, P, H, \mathcal{G})$ where \mathcal{S} is the observation space, \mathcal{A} is the action space, $P(s' | s, a)$ is an unknown dynamics function, H is the maximum horizon, and $\mathcal{G} \subseteq \mathcal{S}$ is the goal space. In goal-conditioned RL, we train a policy $\pi_\theta(a_t | s_t, g)$ to reach goals from the goal space $g \sim \mathcal{G}$ by optimizing the expected cumulative reward $\mathbb{E}_{g \sim \mathcal{G}, \tau \sim (\pi, P)} [\sum_{s \in \tau} R_g(s)]$, where $R_g(s)$ is a reward function defined by some distance metric between goals $g \in \mathcal{G}$ and observations $s \in \mathcal{S}$.

In low-dimensional tasks, one can simply take the reward to be the negative ℓ_2 -distance in the state space (Andrychowicz et al., 2017). However, defining distance metrics is more challenging in high-dimensional spaces, such as images (Yu et al., 2019). Prior work on visual goal-conditioned RL (Nair et al., 2018; Pong et al., 2019) train an additional state representation model, such as a VAE encoder $e^{\text{VAE}} : \mathcal{S} \rightarrow \mathcal{Z}^{\text{VAE}}$. Their methods train a policy over encoded states and goals, and define rewards using ℓ_2 -distance in latent space:

$$R_g(s) = -\|e^{\text{VAE}}(s) - e^{\text{VAE}}(g)\|_2^2.$$

2.2. Weakly-supervised disentangled representations

Our approach leverages weakly-supervised disentangled representation learning in the context of reinforcement learning.

Disentangled representation learning aims to learn interpretable representations of data, where each dimension of the representation measures a distinct *factor of variation*, conditioned on which the data was generated (see Fig. 2 for examples of factors). More formally, consider data-generating processes where $(f_1, \dots, f_K) \in \mathcal{F}$ are the factors of variation, and observations $s \in \mathcal{S}$ are generated from a function $g^* : \mathcal{F} \rightarrow \mathcal{S}$. We would like to learn a disentangled latent representation $e : \mathcal{S} \rightarrow \mathcal{Z}$ such that, for any factor subindices $\mathcal{I} \subseteq [K]$, the subset of latent values $e_{\mathcal{I}}(s) = z_{\mathcal{I}}$ are only influenced by the true factors $f_{\mathcal{I}}$, and conversely, $e_{\mathcal{I}^c}(s) = z_{\mathcal{I}^c}$ are only influenced by $f_{\mathcal{I}^c}$.

We consider a form of weak supervision called *rank pairing*, where data samples $\mathcal{D} := \{(s_1, s_2, y)\}$ consist of pairs of observations $\{s_1, s_2\}$ and weak binary labels $y \in \{0, 1\}^K$, where $y_k = \mathbf{1}(f_k(s_1) < f_k(s_2))$ indicates whether the k th factor value for observation s_1 is smaller than the corresponding factor value for s_2 . Using this data, the weakly-supervised method proposed by Shu et al. (2019) trains an encoder $e : \mathcal{S} \rightarrow \mathcal{Z}$, generator $G : \mathcal{Z} \rightarrow \mathcal{S}$, and discriminator D by optimizing the following losses:

$$\begin{aligned} \min_D \quad & \mathbb{E}_{(s_1, s_2, y) \sim \mathcal{D}} [D(s_1, s_2, y)] \\ & + \mathbb{E}_{z_1, z_2 \sim N(0, I)} (1 - D(G(z_1), G(z_2), y^{\text{fake}})) \\ \max_G \quad & \mathbb{E}_{z_1, z_2 \sim N(0, I)} [D(G(z_1), G(z_2), y^{\text{fake}})] \\ \min_e \quad & \mathbb{E}_{z \sim N(0, I)} [e(z | G(z))] \end{aligned} \quad (1)$$

Shu et al. (2019) showed that this approach is guaranteed to recover the true disentangled representation under mild assumptions. We build upon their work in two respects. First, while Shu et al. (2019) used a balanced and clean dataset, we extend the method to work on significantly less clean data – data from an agent’s observations in a physical world. Second, we show how the learned representations can be used to accelerate RL.

3. The Weakly-Supervised RL Problem

Unlike standard RL, which requires hand-designed reward functions that are often expensive to obtain in complex environments, we aim to design the weakly-supervised RL problem in a way that provides a convenient form of supervision that scales with the collection of offline data. Further, we will require no labels in the loop of reinforcement learning, nor precise segmentations or numerical coordinates to be provided by the human.

Consider an environment with high complexity and large observation space such that it is intractable for an agent to explore the entire state space. Suppose that we have access to an offline dataset of weakly-labeled observations, where the labels capture semantically meaningful properties about the environment that are helpful to solving downstream tasks.

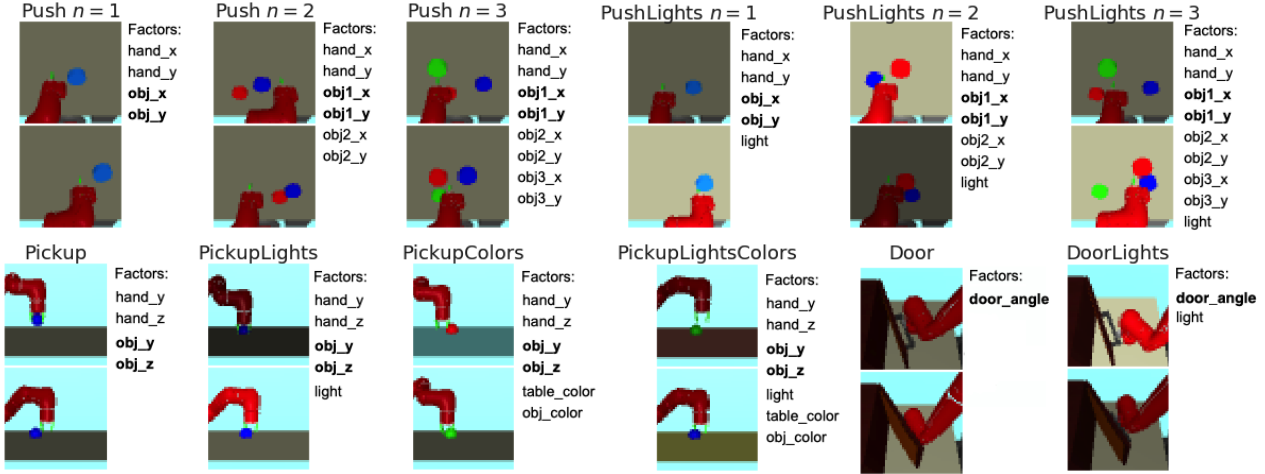


Figure 2: Our method uses weak supervision, like that depicted in this figure, to direct exploration and accelerate learning on visual manipulation tasks of varying complexity. Each data sample consists of a pair of image observations $\{s_1, s_2\}$ and a factor label vector $y \in \{0, 1\}^K$, where $y_k = \mathbf{1}(f_k(s_1) < f_k(s_2))$ indicates whether the k th factor of image s_1 has smaller value than that of image s_2 . Example factors of variation include the gripper position, object positions, brightness, and door angle. Note that we only need to collect labels for the axes of variation that may be relevant for future downstream tasks (see Appendix A.1). In environments with ‘light’ as a factor (e.g., *PushLights*), the lighting conditions change randomly at the start of each episode. In environments with ‘color’ as a factor (e.g., *PickupColors*), both the object color and table color randomly change at the start of each episode. Bolded factors correspond to the user-specified factor indices \mathcal{I} indicating which of the factors are relevant for solving the class of tasks (see Sec. 3)

How can a general-purpose RL agent leverage this dataset to learn new tasks faster? In this section, we formalize this problem statement.

Problem Statement. Assume we are given a weakly-labelled dataset $\mathcal{D} := \{(s_1, s_2, y)\}$, which consists of pairs of observations $\{s_1, s_2\}$ and weak binary labels $y \in \{0, 1\}^K$, where $y_k = \mathbf{1}(f_k(s_1) < f_k(s_2))$ indicates whether the k -th factor value for observation s_1 is smaller than the corresponding factor value for s_2 . Beyond these labels, the user also specifies a subset of indices, $\mathcal{I} \subseteq [K]$, indicating which of the factors $(f_1, \dots, f_K) \in \mathcal{F}$ are relevant for solving a class of tasks. During training, the agent may interact with the environment, but receives no supervision (e.g. no rewards) beyond the weak labels in \mathcal{D} .

At test time, an unknown goal factor $f_{\mathcal{I}}^* \in \mathcal{F}_{\mathcal{I}}$ is sampled, and the agent receives a goal observation, e.g. a goal image, whose factors are equal to $f_{\mathcal{I}}^*$. The agent’s objective is to learn a latent-conditioned RL policy that minimizes the goal distance: $\min_{\pi} \mathbb{E}_{\pi} d(f_{\mathcal{I}}(s), f_{\mathcal{I}}^*)$.

The weakly-supervised RL problem formulated in this section is applicable in many real-world scenarios in which acquiring weak supervision is relatively cheap, e.g. through offline crowd compute, while acquiring demonstrations is expensive and rewards require expertise. For example, consider a vision-based robotic manipulation environment (Fig. 2). The labels in the dataset \mathcal{D} could indicate the relative position of the robot gripper arm between two image observations. The goal factor space $\mathcal{F}_{\mathcal{I}}$ consists of XY-positions of the object that the agent should learn to move

around. Note that we only need to collect labels for the axes of variation that may be relevant for future downstream tasks (see Appendix A.1). At test time, the agent receives a goal image observation, and is evaluated on how closely it can move the object to the goal location.

The next section will develop a RL framework for solving the weakly supervised RL problem. Our experiments (Sec. 5) will investigate whether weak supervision is an economical way to accelerate learning on complex tasks.

4. Weakly-Supervised Control

In this section, we describe a simple training framework for the weakly-supervised RL problem. Our *weakly-supervised control* (WSC) framework consists of two stages: we first learn a disentangled representation from weakly-labelled RL observations, and then use this disentangled space to guide the exploration of goal-conditioned RL along semantically meaningful directions.

4.1. Learning disentangled representations from observations

We build upon the work of Shu et al. (2019) for learning disentangled representations, though, in principle other methods could be used. Their method trains an encoder $e : \mathcal{S} \rightarrow \mathcal{Z}$, generator $G : \mathcal{Z} \rightarrow \mathcal{S}$, and discriminator D by optimizing the losses in Eq. 1. After training the disentanglement model, we discard the discriminator and the generator, and use the encoder to define the goal space and compute distances between states.

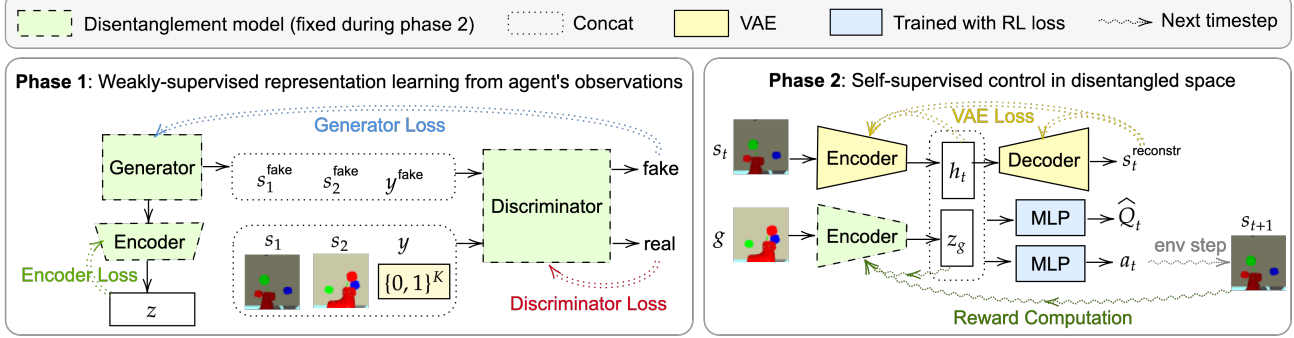


Figure 3: **Weakly-Supervised Control framework.** *Left:* In Phase 1, we use the weakly-labelled dataset $\mathcal{D} = \{(s_1, s_2, y)\}$ to learn a disentangled representation by optimizing the losses in Eq. 1. *Right:* In Phase 2, we use the learned disentangled representation to guide goal generation and define distances. At the start of each episode, the agent samples a latent goal z_g either by encoding a goal image g sampled from the replay buffer, or by sampling directly from the latent goal distribution (Eq. 2). The agent samples actions using the goal-conditioned policy, and defines rewards as the negative ℓ_2 distance between goals and states in the disentangled latent space (Eq. 3).

While Shu et al. (2019) assumes that all combinations of factors are present in the dataset and that data classes are perfectly balanced (i.e., exactly one image for every possible combination of factors), these assumptions usually do not hold for significantly less clean data coming from an agent’s observations in a physical world. For example, not all factor combinations are physically possible to achieve: an object cannot be floating in mid-air without a robot gripper holding it, and two solid objects cannot occupy the same space at the same time. This affects the data distribution: for example, when the robot is holding the object in *Pickup*, there is high correlation between the gripper and object positions. Another issue is partial observability: the agent may lack sensors to observe some aspects of its environment, such as being unable to see through occlusions.

To generate the Sawyer datasets shown in Fig. 2, we corrected the sampled factor combinations to be physically feasible before generating the corresponding image observations in the Mujoco simulator. Furthermore, to reflect the difficulty of collecting a large amount of samples in complex RL environments, we only sampled 256 or 512 images in the training dataset, which is much smaller than the combinatorial size of toy datasets such as dSprites (Matthey et al., 2017) (737,280 images).

Empirically, we found that it is more challenging to learn a disentangled representation on the Sawyer observations (see Table 2), yet we show in Sec. 5 that imperfect disentanglement models can still drastically accelerate training of goal-conditioned policies. In the next section, we describe how we use the learned disentangled space to generate goals, define reward functions, and do directed exploration.

4.2. Structured Goal Generation & Distance Function

In this section, we describe how our method uses the learned disentangled model $e : \mathcal{S} \rightarrow \mathcal{Z}$ and the user-specified factor indices $\mathcal{I} \subseteq [K]$ to train a goal-conditioned policy $\pi(a |$

Algorithm 1 Weakly-Supervised Control

Input: Weakly-labeled dataset \mathcal{D} , factor subindices $\mathcal{I} \subseteq [K]$

- 1: Train disentangled representation $e : \mathcal{S} \mapsto \mathcal{Z}$ using \mathcal{D} .
- 2: Compute $\mathcal{Z}_{\mathcal{I}}^{\min} = \min_{s \in \mathcal{D}} e_{\mathcal{I}}(s)$.
- 3: Compute $\mathcal{Z}_{\mathcal{I}}^{\max} = \max_{s \in \mathcal{D}} e_{\mathcal{I}}(s)$.
- 4: Define $p(\mathcal{Z}_{\mathcal{I}}) := \text{Uniform}(\mathcal{Z}_{\mathcal{I}}^{\min}, \mathcal{Z}_{\mathcal{I}}^{\max})$.
- 5: Initialize replay buffer $\mathcal{R} \leftarrow \emptyset$.
- 6: **for** iteration = 0, 1, ..., **do**
- 7: Sample a goal $z_g \in \mathcal{Z}$ and an initial state s_0 .
- 8: **for** $t = 0, 1, \dots, H - 1$ **do**
- 9: Get action $a_t \sim \pi(s_t, z_g)$.
- 10: Execute action and observe $s_{t+1} \sim p(\cdot | s_t, a_t)$.
- 11: Store (s_t, a_t, s_{t+1}, z_g) into replay buffer \mathcal{R} .
- 12: **for** $t = 0, 1, \dots, H - 1$ **do**
- 13: **for** $j = 0, 1, \dots, J$ **do**
- 14: With probability p , sample $z'_g \sim p(\mathcal{Z}_{\mathcal{I}})$. Otherwise, sample a future state $s' \in \tau_{>t}$ in the current trajectory and compute $z'_g = e_{\mathcal{I}}(s')$.
- 15: Store $(s_t, a_t, s_{t+1}, z'_g)$ into \mathcal{R} .
- 16: **for** $k = 0, 1, \dots, N - 1$ **do**
- 17: Sample $(s, a, s', z_g) \sim \mathcal{R}$.
- 18: Compute $r = R_{z_g}(s') = -\|e_{\mathcal{I}}(s') - z_g\|_2^2$.
- 19: Update actor and critic using (s, a, s', z_g, r) .
- 20: **return** $\pi(a | s, z)$

s, z_g). The agent will propose its own goals to practice, attempt the proposed goals, and use the experience to update its goal-conditioned policy.

Our method defines the goal space to be the learned disentangled latent space $\mathcal{Z}_{\mathcal{I}}$, restricted to the indices in \mathcal{I} . The goal sampling distribution is defined as

$$p(\mathcal{Z}_{\mathcal{I}}) := \text{Uniform}(\mathcal{Z}_{\mathcal{I}}^{\min}, \mathcal{Z}_{\mathcal{I}}^{\max}), \quad (2)$$

where $\mathcal{Z}_{\mathcal{I}}^{\min} = \min_{s \in \mathcal{D}} e_{\mathcal{I}}(s)$ and $\mathcal{Z}_{\mathcal{I}}^{\max} = \max_{s \in \mathcal{D}} e_{\mathcal{I}}(s)$ denote the element-wise min and max latent values.

In each iteration, our method samples latent goals $z_g \in \mathcal{Z}_{\mathcal{I}}$ by either sampling from $p(\mathcal{Z}_{\mathcal{I}})$, or sampling an image observation from the replay buffer and encoding it with the disentangled model, $z_g = e_{\mathcal{I}}(s_g)$. Then, our method at-

Method	$p(\mathcal{Z})$	$R_{z_g}(s')$
RIG	$\mathcal{N}(0, I)$	$-\ e^{\text{VAE}}(s') - z_g\ _2^2$
SkewFit	$p^{\text{skew}}(\mathcal{R})$	$-\ e^{\text{VAE}}(s') - z_g\ _2^2$
WSC	$\text{Uniform}(\mathcal{Z}_{\mathcal{I}}^{\min}, \mathcal{Z}_{\mathcal{I}}^{\max})$	$-\ e_{\mathcal{I}}(s') - z_g\ _2^2$

Table 1: Conceptual comparison between our method weakly-supervised control (WSC), and prior visual goal-conditioned RL methods, with their respective latent goal distributions $p(\mathcal{Z})$ and goal-conditioned reward functions $R_{z_g}(s')$. Our method can be seen as an extension of prior work to the weakly-supervised setting.

tempts this goal by executing the policy to get a trajectory (s_1, a_1, \dots, s_T) . When sampling transitions (s_t, a_t, s_{t+1}, z_g) from the replay buffer for RL training, we use hindsight re-labeling (Andrychowicz et al., 2017) with corrected goals to provide additional training signal. In other words, we sometimes relabel the transition $(s_t, a_t, s_{t+1}, z_g')$ with a corrected goal z_g' , which is sampled from either the goal distribution $p(\mathcal{Z}_{\mathcal{I}})$ in Eq. 2, or from a future state in the current trajectory. Our method defines the reward function as the negative ℓ_2 -distance in the disentangled latent space:

$$r_t := R_{z_g}(s_{t+1}) := -\|e_{\mathcal{I}}(s_{t+1}) - z_g\|_2^2. \quad (3)$$

We summarize our weakly-supervised control (WSC) framework in Fig. 3 and Alg. 1. We start by learning the disentanglement module using the weakly-labelled data. Next, we train the policy with off-policy RL, sampling transitions (s, a, s', z_g) with hindsight relabeling. At termination, our method outputs a goal-conditioned policy $\pi(a | s, z_g)$ which is trained to go to a state that is close to z_g in the disentangled latent space.

5. Experiments

We aim to first and foremost answer our core hypothesis: (1) Does weakly supervised control help guide exploration and learning, for increased performance over prior approaches? Further we also investigate: (2) What is the relative importance of the goal generation mechanism vs. the distance metric used in WSC?, (3) Is weak supervision necessary for learning a disentangled state representation?, (4) Is the policy’s behavior interpretable?, and (5) How much weak supervision is needed to learn a sufficiently-disentangled state representation? Questions (1) through (4) are investigated in this section, while question (5) is studied in Appendix A.1.

To answer these questions, we consider several vision-based, goal-conditioned manipulation tasks of varying complexity, shown in Fig. 2. In the *Push* and *Pickup* environments, the agent’s task is to move a specific object to a goal location. In the *Door* environments, the agent’s task is to open the door to match a goal angle. Both the state and goal observations are 48×48 RGB images.

Comparisons: We compare our method to prior state-of-the-art goal-conditioned RL methods, which are summa-

rized in Table 1. While the original hindsight experience replay (HER) algorithm (Andrychowicz et al., 2017) requires the state space to be disentangled, this assumption does not hold in our problem setting, where the observations are high-dimensional images. Thus, in our experiments, we modified **HER** (Andrychowicz et al., 2017) to sample re-labeled goals from the VAE prior $g \sim \mathcal{N}(0, I)$ and use the negative ℓ_2 -distance between goals and VAE-encoded states as the reward function. **RIG** (Nair et al., 2018) and **SkewFit** (Pong et al., 2019) are extensions of HER that use a modified goal sampling distribution that places higher weight on rarer states. RIG uses MLE to train the VAE, while SkewFit uses data samples from $p^{\text{skew}}(\mathcal{R})$ to train the VAE. For direct comparison, we use the weakly-labeled dataset \mathcal{D} in HER, RIG, and SkewFit to pre-train the VAE, from which goals are sampled.

Additionally, to investigate whether our disentanglement approach for utilizing weak supervision is better than alternative methods, we compare to a variant of SkewFit that optimizes an auxiliary prediction loss on the factor labels, which we refer to as **Skewfit+pred**.

Implementation details: Both the disentanglement model and VAE were pre-trained using the same dataset (size 256 or 512). A separate evaluation dataset of 512 image goals is used to evaluate the policies on visual goal-conditioned tasks. We used soft actor-critic (Haarnoja et al., 2018) as the base RL algorithm. All results are averaged over 5 random seeds. See Appendix B for further details.

5.1. Does weakly supervised control help guide exploration and learning?

Do the disentangled representations acquired by our method guide goal-conditioned policies to explore in more semantically meaningful ways? In Fig. 4, we compare our method to prior state-of-the-art goal-conditioned RL methods on visual goal-conditioned tasks in the Sawyer environments (see Fig. 2). We see that doing directed exploration and goal sampling in a (learned) disentangled latent space is substantially more effective than doing purely unsupervised exploration in VAE latent state space, particularly for environments with increased variety in lighting and appearance.

Then, a natural next question remains: is our disentanglement approach for utilizing weak supervision better than alternative methods? One obvious approach for using supervision is to simply add an auxiliary loss to predict the weak labels from the representation. To this end, we trained a variant of SkewFit where the final hidden layer of the VAE is also trained to optimize an auxiliary prediction loss on the factor labels, which we refer to as ‘Skewfit+pred’. In Fig. 4, we find that Skewfit+pred performs worse than WSC even though it uses stronger supervision (exact labels) compared to WSC. Hence, naive auxiliary losses do not lead to

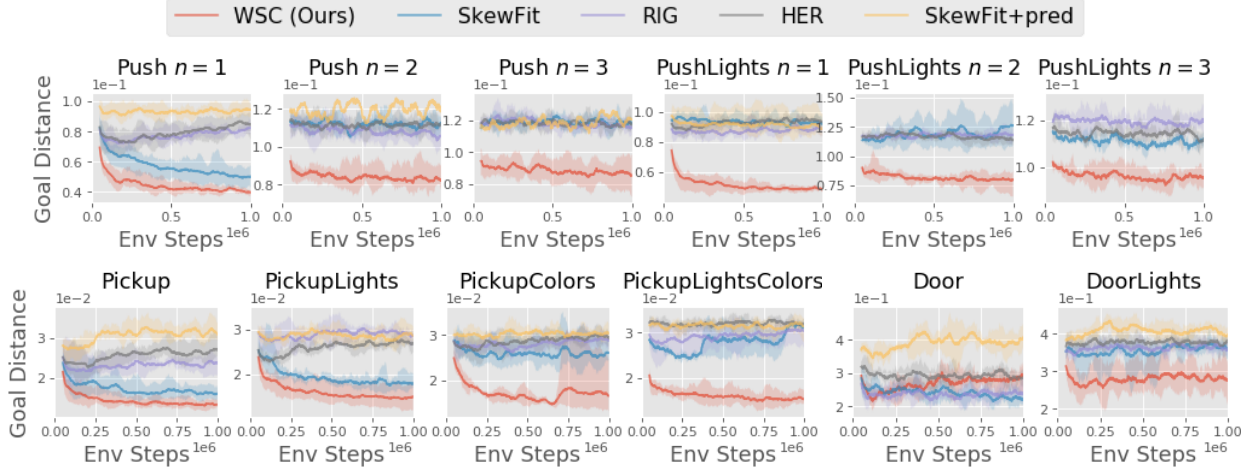


Figure 4: **Performance vs. training steps on visual goal-conditioned tasks.** Weakly-Supervised Control (WSC) learns more quickly than prior state-of-the-art goal-conditioned RL methods (HER, RIG, SkewFit), particularly as the complexity of the environment grows. Thus, we see that doing directed exploration and goal sampling in a (learned) semantically-disentangled latent space can be more effective than doing purely unsupervised exploration in the VAE latent space.

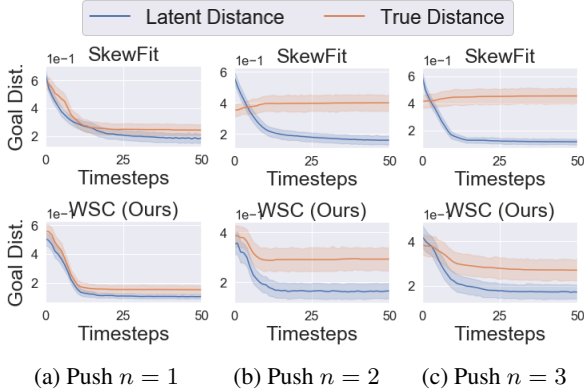


Figure 5: We roll out trained policies on visual goal-conditioned tasks, and compare the latent goal distance vs. the true goal distance between the object and the goal position. As the environment becomes increasingly complex (*Push* with $n \in \{1, 2, 3\}$ objects), the latent distance reward optimized by SkewFit becomes less indicative of the true goal distance, whereas the disentangled distance optimized by our method remains more accurate.

good representations for directing exploration or providing distance metrics. This comparison instead suggests that our approach of disentangling meaningful and irrelevant factor of the environment is important for effectively leveraging weak supervision.

5.2. Ablation: What is the role of distances vs. goals?

Our method uses the representation in two places: for goal-generation (Eq. 2) and for the distance metric (Eq. 3). Our next experiment will study the relative importance of using a disentangled representation in both places. First, we investigate whether the distance metric defined over the learned disentangled representation provides a more accurate signal for the true goal distance. In Fig. 5, we evaluate trained policies on visual goal-conditioned tasks, and compare the

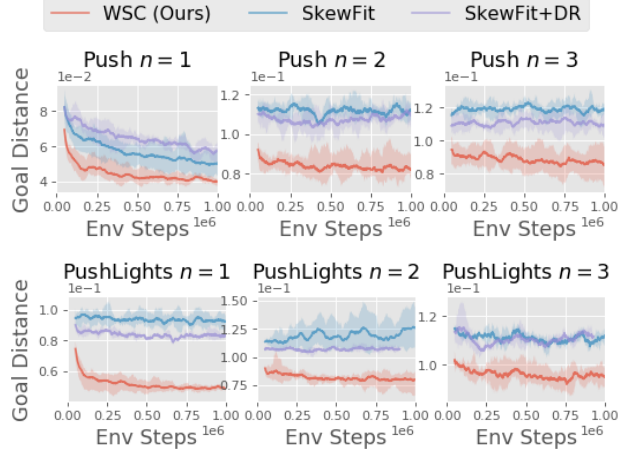


Figure 6: SkewFit+DR is a variant that samples goals in VAE latent space, but uses reward distances in disentangled latent space. We see that the disentangled distance metric can help slightly in harder environments (e.g., *Push* $n = 3$), but the goal generation mechanism of WSC is crucial to achieving efficient exploration.

latent goal distance vs. the true goal distance between the object and the goal position at every timestep. As the environment becomes increasingly complex ($n \in \{1, 2, 3\}$), the latent distance reward optimized by SkewFit becomes less indicative of the true goal distance compared to the disentangled distance optimized by our method. The results suggest that the disentangled representation provide a more accurate reward signal for the training agent.

Next, we tested whether the distance metric in the disentangled space alone is enough to learn goal-conditioned tasks quickly. To do so, we trained a variant of SkewFit that samples latent goals in VAE latent space, but uses distances in disentangled latent space as the reward function. In Fig. 6, we see that the disentangled distance metric can help slightly in harder environments, but underperforms compared to the

full method (WSC) with goal generation in disentangled latent space. Thus, we conclude that both the goal generation mechanism and distance metric of our method are crucial components for enabling efficient exploration.

5.3. Is the learned state representation disentangled?

To see whether weak supervision is necessary to learn state representations that are disentangled, we measure the correlation between true factor values and the latent dimensions of the encoded image in Table 2. For the VAE, we took the latent dimension that has the highest correlation with the true factor value. The results illustrate that unsupervised losses are often insufficient for learning a disentangled representation, and utilizing weak labels in the training process can greatly improve disentanglement, especially as the environment complexity increases.

Env	Factor	Pearson correlation	
		VAE (SkewFit)	WSC (Ours)
Push $n = 1$	hand_x	0.97 ± 0.04	0.97 ± 0.01
	hand_y	0.85 ± 0.07	0.93 ± 0.02
	obj_x	0.78 ± 0.28	0.97 ± 0.01
	obj_y	0.65 ± 0.31	0.95 ± 0.01
Push $n = 3$	hand_x	0.95 ± 0.03	0.98 ± 0.01
	hand_y	0.50 ± 0.33	0.94 ± 0.03
	obj1_x	0.12 ± 0.18	0.96 ± 0.01
	obj1_y	0.15 ± 0.03	0.92 ± 0.02

Table 2: **Is the learned state representation disentangled?** We measure the correlation between the true factor value of the input image vs. the latent dimension of the encoded image on the evaluation dataset. We show the 95% confidence interval over 5 seeds. We find that unsupervised VAEs are often insufficient for learning a disentangled representation.

5.4. Is the policy’s latent space interpretable?

Since our method uses an interpretable latent goal space to generate self-proposed goals and compute rewards for training the policy, we checked whether the learned policy is also semantically meaningful. In Table 3, we measure the correlation between latent goals and the final states of the policy rollout. For various latent goals $z_g \in \mathcal{Z}$, we rolled out the trained policy $\pi(a | s, z_g)$ and compared the final state with the latent goal z_g that the policy was conditioned on (see Section 5.4). For our method, we did a grid sweep over the latent goal values in $[\mathcal{Z}_T^{\min}, \mathcal{Z}_T^{\max}]$. For SkewFit, we took the latent dimensions that have the highest correlations with the true object XY positions, then did a similar grid sweep over the latent goal space. The results show that our method achieves higher Pearson correlation between latent goals and final states, meaning that it learns a more interpretable goal-conditioned policy where the latent goals align directly with the final state of the trajectory rollout.

In Fig. 7, we visualize the trajectories generated by our method’s policy when conditioned on different latent goals

Env	Factor	Pearson correlation	
		SkewFit	WSC (Ours)
Push $n = 1$	obj_x	0.94 ± 0.03	0.95 ± 0.03
	obj_y	0.66 ± 0.17	0.94 ± 0.04
Push $n = 2$	obj1_x	0.59 ± 0.50	0.69 ± 0.37
	obj1_y	0.44 ± 0.68	0.86 ± 0.05
Push $n = 3$	obj1_x	0.44 ± 1.05	0.78 ± 0.11
	obj1_y	0.38 ± 1.44	0.89 ± 0.01

Table 3: **Is the learned policy interpretable?** We investigate whether latent goals z_g align directly with the final state of the trajectory after rolling out $\pi(a | s, z_g)$. We measure the correlation between the true factor value of the final state in the trajectory vs. the corresponding latent dimension of z_g . We show the 95% confidence interval over 5 seeds. Our method attains higher correlation between latent goals and final states, meaning that it learns a more interpretable goal-conditioned policy.

$z_g = (z_1, z_2)$ obtained by doing a grid sweep over the latent space $[\mathcal{Z}_T^{\min}, \mathcal{Z}_T^{\max}]$. The object and gripper were spawned at fixed locations at the start of each trajectory. We see that the latent goal values z_g directly align with the final object position after rolling out the policy $\pi(a | s, z_g)$. In other words, varying each latent goal dimension corresponds to directly changing the object position in the X- or Y-coordinate.

6. Related Work

Reinforcement learning of complex behaviors in rich environments with high-dimensional observations remains an open problem. Many of the successful applications of RL in prior work Silver et al. (2017); Berner et al. (2019); Vinyals et al. (2019); Gu et al. (2017) effectively operate in a regime where the amount of data (i.e., interactions with the environment) dwarfs the complexity of task at hand. Insofar as alternative forms of supervision is the key to success for RL methods, prior work has proposed a number of techniques for making use of various types of ancillary supervision.

A number of prior works incorporate additional supervision beyond rewards to accelerate RL. One common theme is to use the task dynamics itself as supervision, using either forward dynamics (Watter et al., 2015; Finn & Levine, 2017; Hafner et al., 2018; Zhang et al., 2018; Kaiser et al., 2019), some function of forward dynamics (Dosovitskiy & Koltun, 2016), or inverse dynamics (Pathak et al., 2017; Agrawal et al., 2016; Pathak et al., 2018) as a source of labels. Another approach explicitly predicts auxiliary labels (Jaderberg et al., 2016; Shelhamer et al., 2016; Gordon et al., 2018; Dilokthanakul et al., 2019). Compact state representations can also allow for faster learning and planning, and prior work has proposed a number of tools for learning these representations (Mahadevan, 2005; Machado et al., 2017; Finn et al., 2016b; Barreto et al., 2017; Nair et al., 2018; Gelada et al., 2019; Lee et al., 2019a; Yarats et al., 2019). Bengio et al. (2017); Thomas et al. (2017) propose learning representations using an independent controllability metric,

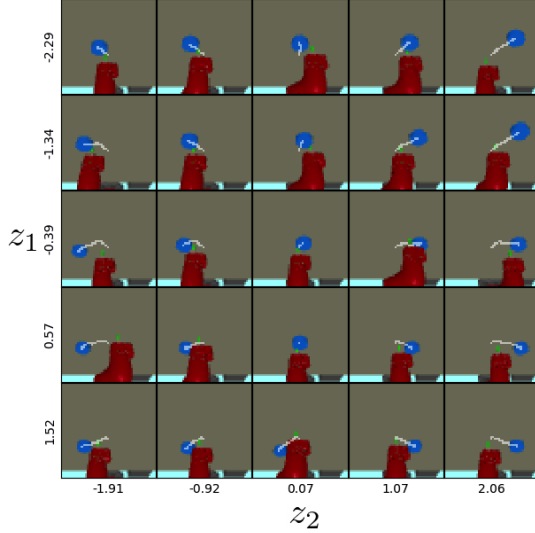


Figure 7: **Interpretable control:** Each of the 5×5 images corresponds to a trajectory generated by our method’s trained policy $\pi(a | s, z_g)$ conditioned on varying latent goals $z_g = (z_1, z_2) \in \mathbb{R}^2$. The blue object always starts at the center of the frame in the beginning of each episode. The white arrow indicate the object’s position throughout the trajectory. The trajectories show that the latent goal values directly align with the direction in which the policy moves the blue object.

but the joint RL and representation learning scheme has proven difficult to scale in environment complexity. Perhaps most related to our method is prior work that directly learns a compact representation of goals (Goyal et al., 2019; Pong et al., 2019; Nachum et al., 2018). Our work likewise learns a low-dimensional representation of goals, but crucially learns it in such a way that we “bake in” a bias towards meaningful goals, thereby avoiding the problem of accidentally discarding salient state dimensions.

Human supervision is an important but expensive aspect of reward design (Hadfield-Menell et al., 2017), and prior work has studied how reward functions might be efficiently elicited from weak supervision. In settings where a human operator can manually control the system, a reward function can be acquired by applying inverse RL on top of human demonstrations (Ratliff et al., 2006; Finn et al., 2016a; Fu et al., 2017; Brown et al., 2019; Ghasemipour et al., 2019). Another technique for sample-efficient reward design is to define rewards in terms of pre-trained classifiers (Xie et al., 2018; Fu et al., 2018; Singh et al., 2019; Vecerik et al., 2019), which might be learned with supervised learning. State marginal distributions, which can be easier to specify in some tasks, have also been used as supervision for RL (Lee et al., 2019b; Ghasemipour et al., 2019). Our method utilizes a much weaker form of supervision than state marginals, which potentially allows it to scale to more complex tasks. A final source of supervisory signal comes in the form of human preferences or rankings (Yaman et al., 2010; Christiano et al., 2017; Brown et al., 2019), where

humans provide weak supervision about which of two behaviors they prefer. Our approach similarly obtains weak supervision from humans, but uses it to acquire a disentangled space for defining many tasks, rather than directly defining a single task reward.

Finally, our approach leverages weakly-supervised disentangled representation learning in the context of reinforcement learning. Learning such semantically-meaningful representations are useful for many downstream tasks that require machine learning models to be human-controllable or interpretable (Gilpin et al., 2018; Lake et al., 2017; van Steenkiste et al., 2019). While there is no canonical definition for disentanglement, several formal definitions have been proposed (Higgins et al., 2018; Shu et al., 2019). Many unsupervised methods for disentangled representation learning (Higgins et al., 2017; Chen et al., 2018; 2016; Kim & Mnih, 2018; Esmaeili et al., 2018) learn a latent-variable model with prior $p(Z)$ and generator g , where $g(Z)$ approximates $g^*(\mathcal{F})$. However, unsupervised methods are generally brittle to hyperparameter settings and, more importantly, do not lead to consistently disentangled latent representations (Locatello et al., 2018). Recently, weakly-supervised disentangled representation learning methods (Chen & Batmanghelich, 2019; Gabbay & Hoshen, 2019; Shu et al., 2019) have been shown to produce more robust disentangled representations than unsupervised methods, without requiring large amounts of supervision.

7. Conclusion

We proposed weak supervision as a means to scalably introduce structure into goal-conditioned reinforcement learning. To leverage the weak supervision, we proposed a simple two phase approach that first learns a disentangled representation and then uses it to guide exploration, propose goals, and inform a distance metric. Our experimental results indicate that our approach, WSC, substantially outperforms self-supervised methods that cannot cope with the breadth of the environments. Further, our comparisons suggest that our disentanglement-based approach is critical for effectively leveraging the weak supervision.

Despite its strong performance, WSC has multiple limitations. While WSC has the ability to leverage weak labels that can be easily collected offline with approaches like crowd compute, WSC requires a user to indicate the factors of variation that are relevant for downstream tasks, which may require expertise. However, we expect the indication of such factors to still require substantially less expert effort than demonstrations or reward specification. Further, our method only uses weak supervision during pre-training, which may produce representations that do not always generalize to new interaction later encountered by the agent. Incorporating weak supervision online, in the loop of RL, could address this issue to improve performance. In such

settings, we expect class imbalance and human-in-the-loop learning to present important, but surmountable challenges.

Looking forward, our results suggest a number of interesting directions for future work. For example, there may be other forms of weak supervision (Shu et al., 2019) that can provide useful signal to the agent, as well as other ways to leverage these labels. Given the promising results in increasingly complex environments, evaluating this approach with robots in real-world environments is an exciting future direction. Overall, we believe that our framework provides a new perspective on supervising the development of general-purpose agents acting in complex environments.

Acknowledgements

We thank Yining Chen, Vitchyr Pong, Ben Poole, and Archit Sharma for helpful discussions and comments. We thank Michael Ahn for help with running the manipulation experiments, and also thank Benjamin Narin, Rafael Rafailov, and Riley DeHaan for help with initial experiments. LL is supported by the National Science Foundation (DGE-1745016). BE is supported by the Fannie and John Hertz Foundation and the National Science Foundation (DGE-1745016). RS is supported by NSF IIS1763562, ONR Grant N000141812861, and US Army. CF is a CIFAR Fellow. Any opinions, findings and conclusions or recommendations expressed in this material are those of the author(s) and do not necessarily reflect the views of the National Science Foundation.

References

- Agrawal, P., Nair, A. V., Abbeel, P., Malik, J., and Levine, S. Learning to poke by poking: Experiential learning of intuitive physics. In *Advances in neural information processing systems*, pp. 5074–5082, 2016.
- Andrychowicz, M., Wolski, F., Ray, A., Schneider, J., Fong, R., Welinder, P., McGrew, B., Tobin, J., Abbeel, O. P., and Zaremba, W. Hindsight experience replay. In *Advances in Neural Information Processing Systems*, pp. 5048–5058, 2017.
- Barreto, A., Dabney, W., Munos, R., Hunt, J. J., Schaul, T., van Hasselt, H. P., and Silver, D. Successor features for transfer in reinforcement learning. In *Advances in neural information processing systems*, pp. 4055–4065, 2017.
- Bengio, E., Thomas, V., Pineau, J., Precup, D., and Bengio, Y. Independently controllable features. *arXiv preprint arXiv:1703.07718*, 2017.
- Berner, C., Brockman, G., Chan, B., Cheung, V., Debiak, P., Denison, C., Farhi, D., Fischer, Q., Hashme, S., Hesse, C., et al. Dota 2 with large scale deep reinforcement learning. *arXiv preprint arXiv:1912.06680*, 2019.
- Brown, D. S., Goo, W., Nagarajan, P., and Niekum, S. Extrapolating beyond suboptimal demonstrations via inverse reinforcement learning from observations. *arXiv preprint arXiv:1904.06387*, 2019.
- Chen, J. and Batmanghelich, K. Weakly supervised disentanglement by pairwise similarities. *arXiv preprint arXiv:1906.01044*, 2019.
- Chen, T. Q., Li, X., Grosse, R. B., and Duvenaud, D. K. Isolating sources of disentanglement in variational autoencoders. In *Advances in Neural Information Processing Systems*, pp. 2610–2620, 2018.
- Chen, X., Duan, Y., Houthoofd, R., Schulman, J., Sutskever, I., and Abbeel, P. Infogan: Interpretable representation learning by information maximizing generative adversarial nets. In *Advances in neural information processing systems*, pp. 2172–2180, 2016.
- Christiano, P. F., Leike, J., Brown, T., Martic, M., Legg, S., and Amodei, D. Deep reinforcement learning from human preferences. In *Advances in Neural Information Processing Systems*, pp. 4299–4307, 2017.
- Dasari, S., Ebert, F., Tian, S., Nair, S., Bucher, B., Schmeckpeper, K., Singh, S., Levine, S., and Finn, C. Robonet: Large-scale multi-robot learning. *arXiv preprint arXiv:1910.11215*, 2019.
- Dilokthanakul, N., Kaplanis, C., Pawlowski, N., and Shanahan, M. Feature control as intrinsic motivation for hierarchical reinforcement learning. *IEEE transactions on neural networks and learning systems*, 30(11):3409–3418, 2019.
- Dosovitskiy, A. and Koltun, V. Learning to act by predicting the future. *arXiv preprint arXiv:1611.01779*, 2016.
- Duan, Y., Andrychowicz, M., Stadie, B., Ho, O. J., Schneider, J., Sutskever, I., Abbeel, P., and Zaremba, W. One-shot imitation learning. In *Advances in neural information processing systems*, pp. 1087–1098, 2017.
- Esmaili, B., Wu, H., Jain, S., Bozkurt, A., Siddharth, N., Paige, B., Brooks, D. H., Dy, J., and van de Meent, J.-W. Structured disentangled representations. *arXiv preprint arXiv:1804.02086*, 2018.
- Finn, C. and Levine, S. Deep visual foresight for planning robot motion. In *2017 IEEE International Conference on Robotics and Automation (ICRA)*, pp. 2786–2793. IEEE, 2017.
- Finn, C., Levine, S., and Abbeel, P. Guided cost learning: Deep inverse optimal control via policy optimization. In *International Conference on Machine Learning*, pp. 49–58, 2016a.
- Finn, C., Tan, X. Y., Duan, Y., Darrell, T., Levine, S., and Abbeel, P. Deep spatial autoencoders for visuomotor learning. In *2016 IEEE International Conference on Robotics and Automation (ICRA)*, pp. 512–519. IEEE, 2016b.
- Finn, C., Abbeel, P., and Levine, S. Model-agnostic meta-learning for fast adaptation of deep networks. In *Proceedings of the 34th International Conference on Machine Learning-Volume 70*, pp. 1126–1135. JMLR. org, 2017.
- Fu, J., Luo, K., and Levine, S. Learning robust rewards with adversarial inverse reinforcement learning. *arXiv preprint arXiv:1710.11248*, 2017.
- Fu, J., Singh, A., Ghosh, D., Yang, L., and Levine, S. Variational inverse control with events: A general framework for data-driven reward definition. In *Advances in Neural Information Processing Systems*, pp. 8538–8547, 2018.

- Gabbay, A. and Hoshen, Y. Latent optimization for non-adversarial representation disentanglement. *arXiv preprint arXiv:1906.11796*, 2019.
- Gelada, C., Kumar, S., Buckman, J., Nachum, O., and Bellemare, M. G. Deepmdp: Learning continuous latent space models for representation learning. *arXiv preprint arXiv:1906.02736*, 2019.
- Ghasemipour, S. K. S., Zemel, R., and Gu, S. A divergence minimization perspective on imitation learning methods. *Conference on Robot Learning (CoRL)*, 2019.
- Gilpin, L. H., Bau, D., Yuan, B. Z., Bajwa, A., Specter, M., and Kagal, L. Explaining explanations: An overview of interpretability of machine learning. In *2018 IEEE 5th International Conference on data science and advanced analytics (DSAA)*, pp. 80–89. IEEE, 2018.
- Gordon, D., Kembhavi, A., Rastegari, M., Redmon, J., Fox, D., and Farhadi, A. Iqa: Visual question answering in interactive environments. In *Proceedings of the IEEE Conference on Computer Vision and Pattern Recognition*, pp. 4089–4098, 2018.
- Goyal, A., Islam, R., Strouse, D., Ahmed, Z., Botvinick, M., Larochelle, H., Levine, S., and Bengio, Y. Infobot: Transfer and exploration via the information bottleneck. *arXiv preprint arXiv:1901.10902*, 2019.
- Gu, S., Holly, E., Lillicrap, T., and Levine, S. Deep reinforcement learning for robotic manipulation with asynchronous off-policy updates. In *2017 IEEE international conference on robotics and automation (ICRA)*, pp. 3389–3396. IEEE, 2017.
- Haarnoja, T., Zhou, A., Abbeel, P., and Levine, S. Soft actor-critic: Off-policy maximum entropy deep reinforcement learning with a stochastic actor. *arXiv preprint arXiv:1801.01290*, 2018.
- Hadfield-Menell, D., Milli, S., Abbeel, P., Russell, S. J., and Dragan, A. Inverse reward design. In *Advances in neural information processing systems*, pp. 6765–6774, 2017.
- Hafner, D., Lillicrap, T., Fischer, I., Villegas, R., Ha, D., Lee, H., and Davidson, J. Learning latent dynamics for planning from pixels. *arXiv preprint arXiv:1811.04551*, 2018.
- Hausman, K., Springenberg, J. T., Wang, Z., Heess, N., and Riedmiller, M. Learning an embedding space for transferable robot skills. 2018.
- Hazan, E., Kakade, S. M., Singh, K., and Van Soest, A. Provably efficient maximum entropy exploration. *arXiv preprint arXiv:1812.02690*, 2018.
- Higgins, I., Matthey, L., Pal, A., Burgess, C., Glorot, X., Botvinick, M., Mohamed, S., and Lerchner, A. beta-vae: Learning basic visual concepts with a constrained variational framework. *Iclr*, 2(5):6, 2017.
- Higgins, I., Amos, D., Pfau, D., Racaniere, S., Matthey, L., Rezende, D., and Lerchner, A. Towards a definition of disentangled representations. *arXiv preprint arXiv:1812.02230*, 2018.
- Jaderberg, M., Mnih, V., Czarnecki, W. M., Schaul, T., Leibo, J. Z., Silver, D., and Kavukcuoglu, K. Reinforcement learning with unsupervised auxiliary tasks. *arXiv preprint arXiv:1611.05397*, 2016.
- Kaelbling, L. P. Learning to achieve goals. In *IJCAI*, pp. 1094–1099. Citeseer, 1993.
- Kaiser, L., Babaeizadeh, M., Milos, P., Osinski, B., Campbell, R. H., Czechowski, K., Erhan, D., Finn, C., Kozakowski, P., Levine, S., et al. Model-based reinforcement learning for atari. *arXiv preprint arXiv:1903.00374*, 2019.
- Kim, H. and Mnih, A. Disentangling by factorising. *arXiv preprint arXiv:1802.05983*, 2018.
- Lake, B. M., Ullman, T. D., Tenenbaum, J. B., and Gershman, S. J. Building machines that learn and think like people. *Behavioral and brain sciences*, 40, 2017.
- Laskey, M., Lee, J., Fox, R., Dragan, A., and Goldberg, K. Dart: Noise injection for robust imitation learning. *arXiv preprint arXiv:1703.09327*, 2017.
- Lee, A. X., Nagabandi, A., Abbeel, P., and Levine, S. Stochastic latent actor-critic: Deep reinforcement learning with a latent variable model. *arXiv preprint arXiv:1907.00953*, 2019a.
- Lee, L., Eysenbach, B., Parisotto, E., Xing, E., Levine, S., and Salakhutdinov, R. Efficient exploration via state marginal matching. *arXiv preprint arXiv:1906.05274*, 2019b.
- Locatello, F., Bauer, S., Lucic, M., Rätsch, G., Gelly, S., Schölkopf, B., and Bachem, O. Challenging common assumptions in the unsupervised learning of disentangled representations. *arXiv preprint arXiv:1811.12359*, 2018.
- Machado, M. C., Bellemare, M. G., and Bowling, M. A laplacian framework for option discovery in reinforcement learning. In *Proceedings of the 34th International Conference on Machine Learning-Volume 70*, pp. 2295–2304. JMLR. org, 2017.
- Mahadevan, S. Proto-value functions: Developmental reinforcement learning. In *Proceedings of the 22nd international conference on Machine learning*, pp. 553–560. ACM, 2005.
- Mandlekar, A., Zhu, Y., Garg, A., Booher, J., Spero, M., Tung, A., Gao, J., Emmons, J., Gupta, A., Orbay, E., et al. Roboturk: A crowdsourcing platform for robotic skill learning through imitation. *arXiv preprint arXiv:1811.02790*, 2018.
- Matthey, L., Higgins, I., Hassabis, D., and Lerchner, A. dsprites: Disentanglement testing sprites dataset. <https://github.com/deepmind/dsprites-dataset/>, 2017.
- Nachum, O., Gu, S., Lee, H., and Levine, S. Near-optimal representation learning for hierarchical reinforcement learning. *arXiv preprint arXiv:1810.01257*, 2018.
- Nair, A. V., Pong, V., Dalal, M., Bahl, S., Lin, S., and Levine, S. Visual reinforcement learning with imagined goals. In *Advances in Neural Information Processing Systems*, pp. 9191–9200, 2018.
- Pathak, D., Agrawal, P., Efros, A. A., and Darrell, T. Curiosity-driven exploration by self-supervised prediction. In *Proceedings of the IEEE Conference on Computer Vision and Pattern Recognition Workshops*, pp. 16–17, 2017.
- Pathak, D., Mahmoudieh, P., Luo, G., Agrawal, P., Chen, D., Shentu, Y., Shelhamer, E., Malik, J., Efros, A. A., and Darrell, T. Zero-shot visual imitation. In *Proceedings of the IEEE Conference on Computer Vision and Pattern Recognition Workshops*, pp. 2050–2053, 2018.

- Pong, V., Gu, S., Dalal, M., and Levine, S. Temporal difference models: Model-free deep rl for model-based control. *arXiv preprint arXiv:1802.09081*, 2018.
- Pong, V. H., Dalal, M., Lin, S., Nair, A., Bahl, S., and Levine, S. Skew-fit: State-covering self-supervised reinforcement learning. *arXiv preprint arXiv:1903.03698*, 2019.
- Pugh, J. K., Soros, L. B., and Stanley, K. O. Quality diversity: A new frontier for evolutionary computation. *Frontiers in Robotics and AI*, 3:40, 2016.
- Ratliff, N. D., Bagnell, J. A., and Zinkevich, M. A. Maximum margin planning. In *Proceedings of the 23rd international conference on Machine learning*, pp. 729–736, 2006.
- Schaul, T., Horgan, D., Gregor, K., and Silver, D. Universal value function approximators. In *International conference on machine learning*, pp. 1312–1320, 2015.
- Shelhamer, E., Mahmoudieh, P., Argus, M., and Darrell, T. Loss is its own reward: Self-supervision for reinforcement learning. *arXiv preprint arXiv:1612.07307*, 2016.
- Shu, R., Chen, Y., Kumar, A., Ermon, S., and Poole, B. Weakly supervised disentanglement with guarantees. *arXiv preprint arXiv:1910.09772*, 2019.
- Silver, D., Hubert, T., Schrittwieser, J., Antonoglou, I., Lai, M., Guez, A., Lanctot, M., Sifre, L., Kumaran, D., Graepel, T., et al. Mastering chess and shogi by self-play with a general reinforcement learning algorithm. *arXiv preprint arXiv:1712.01815*, 2017.
- Singh, A., Yang, L., Hartikainen, K., Finn, C., and Levine, S. End-to-end robotic reinforcement learning without reward engineering. *arXiv preprint arXiv:1904.07854*, 2019.
- Stanley, K. O. and Miikkulainen, R. Evolving neural networks through augmenting topologies. *Evolutionary computation*, 10(2):99–127, 2002.
- Thomas, V., Pondard, J., Bengio, E., Sarfati, M., Beaudoin, P., Meurs, M.-J., Pineau, J., Precup, D., and Bengio, Y. Independently controllable features. *arXiv preprint arXiv:1708.01289*, 2017.
- van Steenkiste, S., Locatello, F., Schmidhuber, J., and Bachem, O. Are disentangled representations helpful for abstract visual reasoning? In *Advances in Neural Information Processing Systems*, pp. 14222–14235, 2019.
- Vecerik, M., Sushkov, O., Barker, D., Rothörl, T., Hester, T., and Scholz, J. A practical approach to insertion with variable socket position using deep reinforcement learning. In *2019 International Conference on Robotics and Automation (ICRA)*, pp. 754–760. IEEE, 2019.
- Vinyals, O., Babuschkin, I., Czarnecki, W. M., Mathieu, M., Dudzik, A., Chung, J., Choi, D. H., Powell, R., Ewalds, T., Georgiev, P., et al. Grandmaster level in starcraft ii using multi-agent reinforcement learning. *Nature*, 575(7782):350–354, 2019.
- Watter, M., Springenberg, J., Boedecker, J., and Riedmiller, M. Embed to control: A locally linear latent dynamics model for control from raw images. In *Advances in neural information processing systems*, pp. 2746–2754, 2015.
- Xie, A., Singh, A., Levine, S., and Finn, C. Few-shot goal inference for visuomotor learning and planning. *arXiv preprint arXiv:1810.00482*, 2018.
- Yaman, F., Walsh, T. J., Littman, M. L., et al. Learning lexicographic preference models. In *Preference learning*, pp. 251–272. Springer, 2010.
- Yarats, D., Zhang, A., Kostrikov, I., Amos, B., Pineau, J., and Fergus, R. Improving sample efficiency in model-free reinforcement learning from images. *arXiv preprint arXiv:1910.01741*, 2019.
- Yu, T., Shevchuk, G., Sadigh, D., and Finn, C. Unsupervised visuomotor control through distributional planning networks. *arXiv preprint arXiv:1902.05542*, 2019.
- Zhang, M., Vikram, S., Smith, L., Abbeel, P., Johnson, M. J., and Levine, S. Solar: Deep structured latent representations for model-based reinforcement learning. *arXiv preprint arXiv:1808.09105*, 2018.

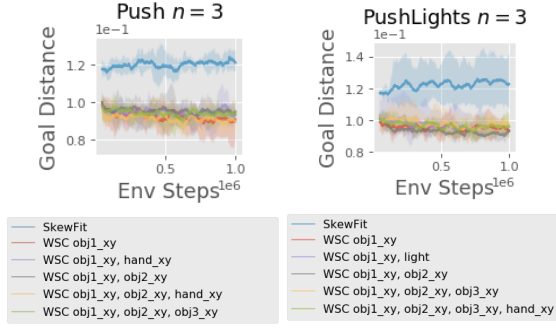


Figure 8: **How many factors of variation need to be labelled?** WSC outperforms SkewFit even without being provided weak labels for task-irrelevant factors, such as hand position and lighting.

A. Additional Experimental Results

A.1. How much weak supervision is needed?

Our method relies on learning a disentangled representation from weakly-labelled data, $\mathcal{D} = \{(s_1^{(i)}, s_2^{(i)}, y^{(i)})\}_{i=1}^N$. However, the total possible number of pairwise labels for each factor of variation is $N = \binom{M}{2}$, where $M \in \{256, 512\}$ is the number of images in the dataset. In this section, we investigate how much weak supervision is needed to learn a sufficiently-disentangled state representation such that it helps supervise goal-conditioned RL.

How many factors of variation need to be labeled?

There can be many axes of variation in an image observation, especially as the complexity of the environment grows. For example, the *PushLights* environment with $n = 3$ objects has nine factors of variation, including the positions of the robot arm and objects, and lighting (see Figure 2).

In Figure 8, we investigate whether WSC requires weak labels for all or some of the factors of variation. To do so, we compared the performance of WSC as we vary the set of factors of variation that are weakly-labelled in the dataset \mathcal{D} . We see that WSC performs well even when weak labels are not provided for task-irrelevant factors of variation, such as hand position and lighting.

How many weak labels are needed? In Table 4, we evaluate the quality of the learned disentangled representation model as we vary the number of weak labels, M . We measure disentanglement by evaluating the Pearson correlation between the true factor value compared to the latent dimension. We observe that, even with only 1024 pairwise labels, the resulting representation has a good degree of disentanglement, i.e. Pearson correlation of 0.8 or higher.

In Figure 9, we evaluate the downstream performance of our method on visual goal-conditioned tasks as we vary the number of weak labels. We see that our method outperforms SkewFit when provided at least 1024, 1024, 256, and 128 weak labels for *Push* $n = 1$, *PushLights* $n = 3$, *PickupLightsColors*, and *DoorLights*, respectively. Further,

we find that 1024 pairwise labels is generally sufficient for good performance on all domains.

A.2. Latent policy visualizations: WSC vs. SkewFit

We provide additional visualizations of the policy’s latent space on more complex environments, previously discussed in Section 5.4. In Figure 10, we compare the latent space of policies trained by WSC and SkewFit. We see that our method produces a more semantically-meaningful goal-conditioned policy, where the latent goal values directly align with the final position of the target object. The difference between WSC and SkewFit grows larger as we increase the complexity of the environment (i.e., increase the number of objects from one to three).

B. Experimental Details

In this section, we provide implementation details for the experimental setup and algorithms.

B.1. Dataset generation

Both the training and test datasets were generated from the same distribution, and each consists of 256 or 512 images (see Table 5). To generate the Sawyer datasets shown in Fig. 2, we first sampled each factor value uniformly within their respective range, then corrected the factors to be physically feasible before generating the corresponding image observations in the Mujoco simulator. In *Push* environments with $n > 1$ objects, the object positions were corrected to avoid collision. In *Pickup* environments, we sampled the object position on the ground ($\text{obj_z}=0$) with 0.8 probability, and otherwise placed the object in the robot gripper ($\text{obj_z} \geq 0$). In *Door* environments, the gripper position was corrected to avoid collision with the door.

B.2. Environments

Eval metric: At test-time, all RL methods only have access to the test goal image, and is evaluated on the true goal distance. In *Push* and *Pickup*, the true goal distance is defined as the ℓ_2 -distance between the current object position and the goal position. In *Push* environments with $n > 1$ objects, we only consider the goal distance for the blue object, and ignore the red and green objects (which are distractor objects to make the task more difficult). In *Door* environments, the true goal distance is defined as the distance between the current door angle and the goal angle value.

Domain randomization: To further increase task complexity, we randomized the dynamics of some environments. In environments with ‘light’ as a factor (*PushLights*, *PickupLights*, *PickupLightsColors*, *DoorLights*), the lighting changes randomly at the start of each episode, with diffuse values sampled from $\text{Uniform}(0.2, 0.8)$. In environments with ‘color’ as a factor (*PickupColors*, *PickupLightsColors*), both the object color and table color are randomly at the start of each episode (from 5 table colors and 3 object colors).

N	PushLights $n = 3$								
	hand.x	hand.y	obj1.x	obj1.y	obj2.x	obj2.y	obj3.x	obj3.y	light
128	0.79 \pm 0.04	0.64 \pm 0.05	0.44 \pm 0.08	0.32 \pm 0.05	0.60 \pm 0.03	0.51 \pm 0.05	0.49 \pm 0.07	0.41 \pm 0.06	0.86 \pm 0.04
256	0.87 \pm 0.02	0.75 \pm 0.05	0.58 \pm 0.04	0.57 \pm 0.04	0.60 \pm 0.04	0.66 \pm 0.03	0.65 \pm 0.07	0.50 \pm 0.06	0.90 \pm 0.02
512	0.93 \pm 0.01	0.86 \pm 0.01	0.71 \pm 0.03	0.70 \pm 0.05	0.70 \pm 0.04	0.58 \pm 0.05	0.76 \pm 0.04	0.67 \pm 0.05	0.85 \pm 0.04
1024	0.97 \pm 0.01	0.91 \pm 0.01	0.86 \pm 0.01	0.81 \pm 0.02	0.83 \pm 0.02	0.80 \pm 0.03	0.83 \pm 0.03	0.80 \pm 0.02	0.94 \pm 0.02
2048	0.98 \pm 0.00	0.94 \pm 0.01	0.89 \pm 0.01	0.87 \pm 0.03	0.87 \pm 0.01	0.86 \pm 0.02	0.86 \pm 0.02	0.84 \pm 0.02	0.92 \pm 0.01
4096	0.97 \pm 0.00	0.94 \pm 0.01	0.93 \pm 0.01	0.88 \pm 0.01	0.90 \pm 0.01	0.88 \pm 0.02	0.91 \pm 0.01	0.85 \pm 0.01	0.95 \pm 0.00
VAE	0.00 \pm 0.00	0.00 \pm 1.00	0.02 \pm 2.00	0.00 \pm 3.00	0.01 \pm 4.00	0.01 \pm 5.00	0.02 \pm 6.00	0.02 \pm 7.00	0.02 \pm 8.00

N	PickupLightsColors					DoorLights	
	hand.y	hand.z	obj.y	obj.z	light	door.angle	light
128	0.94 \pm 1.00	0.91 \pm 2.00	0.72 \pm 4.00	0.31 \pm 5.00	0.88 \pm 6.00	0.43 \pm 7.00	0.62 \pm 8.00
256	0.95 \pm 1.00	0.96 \pm 2.00	0.85 \pm 4.00	0.47 \pm 5.00	0.95 \pm 6.00	0.62 \pm 7.00	0.77 \pm 8.00
512	0.96 \pm 1.00	0.97 \pm 2.00	0.91 \pm 4.00	0.61 \pm 5.00	0.97 \pm 6.00	0.79 \pm 7.00	0.82 \pm 8.00
1024	0.95 \pm 1.00	0.96 \pm 2.00	0.94 \pm 4.00	0.69 \pm 5.00	0.97 \pm 6.00	0.87 \pm 7.00	0.92 \pm 8.00
2048	0.95 \pm 1.00	0.98 \pm 2.00	0.95 \pm 4.00	0.75 \pm 5.00	0.96 \pm 6.00	0.90 \pm 7.00	0.93 \pm 8.00
4096	0.95 \pm 1.00	0.96 \pm 2.00	0.94 \pm 4.00	0.80 \pm 5.00	0.96 \pm 6.00	0.89 \pm 7.00	0.96 \pm 8.00
VAE	0.08 \pm 0.00	0.25 \pm 1.00	0.07 \pm 2.00	0.09 \pm 3.00	0.24 \pm 4.00	0.09 \pm 5.00	0.04 \pm 6.00

Table 4: **How many weak labels are needed to learn a sufficiently-disentangled state representation?** We trained disentangled representations on varying numbers of weakly-labelled data samples $\{(s_1^{(i)}, s_2^{(i)}, y^{(i)})\}_{i=1}^N$ ($N \in \{128, 256, \dots, 4096\}$), then evaluated how well they disentangled the true factors of variation in the data. On the evaluation dataset, we measure the Pearson correlation between the true factor value of the input image vs. the latent dimension of the encoded image. For the VAE (obtained from SkewFit), we took the latent dimension that has the highest correlation with the true factor value. We report the 95% confidence interval over 5 seeds. Even with a small amount of weak supervision (e.g. around 1024 labels), we are able to attain a representation with good disentanglement.

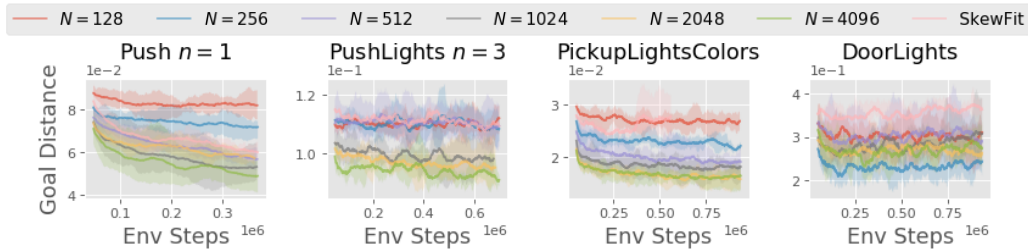


Figure 9: **How many weak labels are needed to help visual goal-conditioned RL?** We evaluate the performance of our method (WSC) on visual goal-conditioned tasks as we vary the number of weak pairwise labels $N \in \{128, 256, \dots, 4096\}$. We find that 1024 pairwise labels is generally sufficient for good performance on all domains.

B.3. Algorithm implementation details

Disentangled representation. We describe the disentangled model network architecture in Table 6, which was slightly modified from (Shu et al., 2019) to be trained on 48×48 image observations from the Sawyer manipulation environments. The encoder is not trained jointly with the generator, and is only trained on generated data from $G(z)$ (see Eq. 1). All models were trained using Adam optimizer with $\beta_1 = 0.5$, $\beta_2 = 0.999$, learning rate $1e-3$, and batch size 64 for $1e5$ iterations. The learned disentangled representation is fixed during RL training (Phase 2 in Figure 3).

Goal-conditioned RL. The policy and Q-functions each are feedforward networks with (400, 300) hidden sizes and ReLU activation. All policies were trained using Soft Actor-Critic (Haarnoja et al., 2018) with batch size 1024, discount factor 0.99, reward scale 1, and replay buffer size $1e5$. The episodic horizon length was set to 50 for *Push* and *Pickup* environments, and 100 for *Door* environments. We used the default hyperparameters for SkewFit from (Pong et al., 2019), which uses 10 latent samples for estimating density. For WSC, we relabelled between 0.2 and 0.5 goals with $z_g \sim p(\mathcal{Z}_I)$ (see Table 5). All RL methods (WSC, SkewFit, RIG, HER) relabel 20% of goals with a future state in the

trajectory. SkewFit and RIG additionally relabel 50% of goals with $z_g \sim p^{\text{skew}}(s)$ and $z_g \sim \mathcal{N}(0, I)$, respectively.

VAE. The VAE was pre-trained on the images from the weakly-labelled dataset for 1000 epochs, then trained on environment observations during RL training. We trained the VAE and the policy separately as was done in (Pong et al., 2019), and found that jointly training them end-to-end did not perform well. We used learning rate $1e-3$, KL regularization coefficient $\beta \in \{20, 30\}$, and batch size 128. The VAE network architecture and hyperparameters are summarized in Table 7.

SkewFit+pred (Section 5.1): We added a dense layer on top of the VAE encoder to predict the factor values, and added a MSE prediction loss to the β -VAE loss. We also tried using the last hidden layer of the VAE encoder instead of the encoder output, but found that it did not perform well.

SkewFit+DR (Figure 6): We tried with and without adding the VAE distance reward to the disentangled reward $R_{z_g}(s)$ in Eq. 3, and report the best α^{VAE} in Table 5:

$$R^{\text{DR}}(s) = R_{z_g}(s) - \alpha^{\text{VAE}} \|e^{\text{VAE}}(s) - z_g^{\text{VAE}}\| \quad (4)$$

Computing infrastructure: Experiments were ran on GTX 1080 Ti, Tesla P100, and Tesla K80 GPU’s.

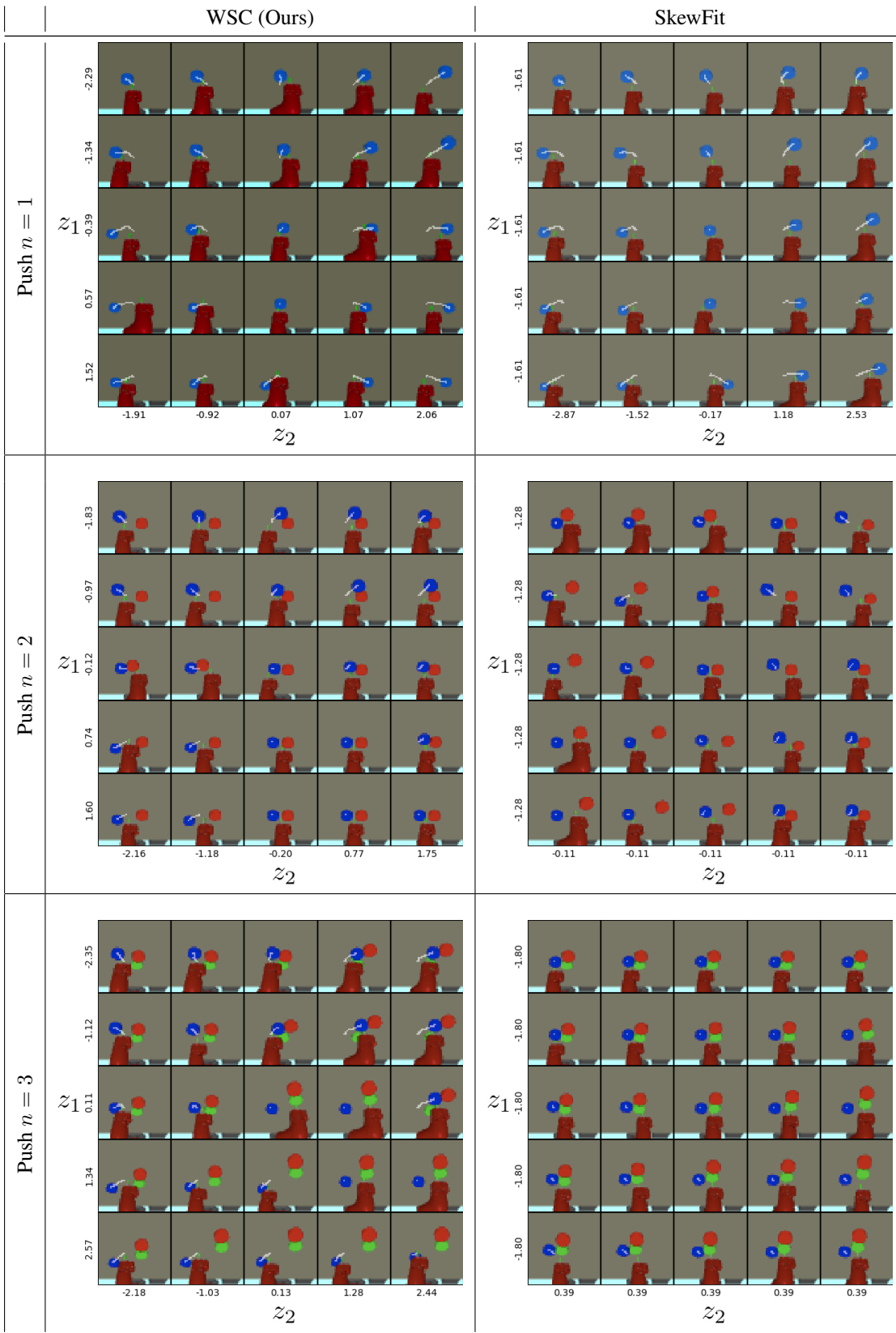


Figure 10: **Interpretable control:** Trajectories generated by WSC (*left*) and SkewFit (*right*), where the policies are conditioned on varying latent goals $(z_1, z_2) \in \mathbb{R}^2$. For SkewFit, we varied the latent dimensions that have the highest correlation with the object’s XY-position, and kept the remaining latent dimensions fixed. The blue object always starts at the center of the frame in the beginning of each episode. The white lines indicate the target object’s position throughout the trajectory. For WSC, we see that the latent goal values directly align with the direction in which the policy moves the blue object.

Environment	M	Factors (User-specified factor indices are bolded)	WSC p_{goal}	α^{DR}
Push $n = 1$	256	hand_x, hand_y, obj_x , obj_y	0.2	1
Push $n = 2$	256	hand_x, hand_y, obj1_x , obj1_y , obj2_x, obj2_y	0.3	1
Push $n = 3$	512	hand_x, hand_y, obj1_x , obj1_y , obj2_x, obj2_y, obj3_x, obj3_y	0.4	0
PushLights $n = 1$	256	hand_x, hand_y, obj_x , obj_y , light	0.4	1
PushLights $n = 2$	512	hand_x, hand_y, obj1_x , obj1_y , obj2_x, obj2_y, light	0.4	1
PushLights $n = 3$	512	hand_x, hand_y, obj1_x , obj1_y , obj2_x, obj2_y, obj3_x, obj3_y, light	0.5	0
Pickup	512	hand_y, hand_z, obj_y , obj_z	0.4	–
PickupLights	512	hand_y, hand_z, obj_y , obj_z , light	0.3	–
PickupColors	512	hand_y, hand_z, obj_y , obj_z , table_color, obj_color	0.4	–
PickupLightsColors	512	hand_y, hand_z, obj_y , obj_z , light, table_color, obj_color	0.3	–
Door	512	door_angle	0.3	–
DoorLights	512	door_angle , light	0.5	–

Table 5: **Environment-specific hyperparameters:** M is the number of training images. “WSC p_{goal} ” is the percentage of goals that are relabelled with $z_g \sim p(\mathcal{Z}_T)$ in WSC. α^{DR} is the VAE reward coefficient for SkewFit+DR in Eq. 4.

Probabilistic Gaussian encoder $e(z s) = \mathcal{N}(z; \mu(s), \sigma(s))$	Generator $G(z)$	Discriminator body	Discriminator $D(s_1, s_2, y)$
Input: $48 \times 48 \times 3$ image	Input: $z \in \mathbb{R}^K$	Input: $48 \times 48 \times 3$ image	Input: Weakly-labelled data
4×4 Conv., 32 ch., stride 2	128 Dense layer	4×4 Conv., 32 ch., stride 2	s_1 s_2 y
Spectral norm	Batch norm	Spectral norm	$\{\pm 1\}^K$
LeakyReLU	ReLU	LeakyReLU	
4×4 Conv., 32 ch., stride 2	$3 \cdot 3 \cdot 64$ Dense layer	4×4 Conv., 32 ch., stride 2	
Spectral norm	Batch norm	Spectral norm	
LeakyReLU	ReLU	LeakyReLU	
4×4 Conv., 64 ch., stride 2	Reshape $3 \times 3 \times 64$	4×4 Conv., 64 ch., stride 2	
Spectral norm	3×3 Conv., 32 ch., stride 2	Spectral norm	
LeakyReLU	Batch norm	LeakyReLU	
4×4 Conv., 64 ch., stride 2	3×3 Conv., 16 ch., stride 2	4×4 Conv., 64 ch., stride 2	
Spectral norm	Batch norm	Spectral norm	
LeakyReLU	LeakyReLU	LeakyReLU	
Flatten	Sigmoid	Flatten	
128 Dense layer	6×6 Conv., 3 ch., stride 4	256 Dense layer	
Spectral norm	Batch norm	Spectral norm	
LeakyReLU		LeakyReLU	
$2 \cdot K$ Dense layer	Output: $48 \times 48 \times 3$ image	256 Dense layer	
Output: $\mu, \sigma \in \mathbb{R}^K$		Spectral norm	
		LeakyReLU	
		Output: Hidden layer h	
			Discriminator body
			h_1 h_2
			$-$ $*$
			Dense layer
			Spectral norm
			$o_1 + o_2 + o^{\text{diff}}$
			Output: Prediction
			$o_1 + o_2 + o^{\text{diff}} \in [0, 1]$

Table 6: **Disentangled representation model architecture:** We slightly modified the disentangled model architecture from (Shu et al., 2019) for 48×48 image observations. The discriminator body is applied separately to s_1 and s_2 to compute the unconditional logits o_1 and o_2 respectively, and the conditional logit is computed as $o^{\text{diff}} = y \cdot (h_1 - h_2)$, where h_1, h_2 are the hidden layers and $y \in \{\pm 1\}$.

VAE encoder $\mathcal{N}(z; \mu(s), \sigma(s))$	VAE decoder	Best latent dim L^{VAE}		
Input: $48 \times 48 \times 3$ image	Input: $z \in \mathbb{R}^{L^{\text{VAE}}}$	Env	β	WSC SkewFit, RIG, HER
5×5 Conv., 16 ch., stride 2	$3 \cdot 3 \cdot 64$ Dense layer	Push	20	256 4
ReLU	Reshape $3 \times 3 \times 64$	Pickup	30	256 16
3×3 Conv., 32 ch., stride 2	3×3 Conv., 32 ch., stride 2	Door	20	256 16
ReLU	ReLU			
3×3 Conv., 64 ch., stride 2	3×3 Conv., 16 ch., stride 2			
ReLU	ReLU			
Flatten	Output: $48 \times 48 \times 3$ image			
$2 \cdot L^{\text{VAE}}$ Dense layer				
Output: $\mu, \sigma \in \mathbb{R}^{L^{\text{VAE}}}$				

Table 7: **VAE architecture & hyperparameters:** β is the KL regularization coefficient in the β -VAE loss. We found that a smaller VAE latent dim $L^{\text{VAE}} \in \{4, 16\}$ worked best for SkewFit, RIG, and HER (which use the VAE for both hindsight relabelling and for the actor & critic networks), but a larger dim $L^{\text{VAE}} = 256$ benefitted WSC (which only uses the VAE for the actor & critic networks).